# The effects of $CO_2$-brine rheology on leakage processes in geologic carbon sequestration

Shibo Wang[1] and Andres F. Clarens[1]

Received 29 July 2011; revised 15 June 2012; accepted 23 June 2012; published 24 August 2012.

[1] Leakage from geologic carbon sequestration (GCS) sites is inherently challenging to study because $CO_2$, driven by buoyant forces, travels over long distances, undergoing phase changes and encountering numerous connate brine and formation chemistries as it rises to the surface. This work explores the effect that $CO_2$ has on the rheological properties of brine solutions over a range of GCS-relevant temperature, pressure, ionic strength, and shear conditions. Under the fluid-liquid equilibrium conditions that prevail in the deep subsurface, viscosity of $CO_2$-brine mixtures was found to be a function of temperature and pressure alone. Once leakage conditions ensue, discrete $CO_2$ bubbles form in brine, resulting in the vapor-liquid equilibrium (VLE), and these mixtures exhibit complex linear viscoelastic, time dependent, and thixotropic behavior. The presence of $CO_{2(g)}$ bubbles on the flow of the bulk fluid could have important impacts on impeding (via shear drag force) leakage depending on the geometrical, geochemical and geophysical characteristics of a storage site. Under VLE conditions, the effective viscosity of $CO_2$-brine mixtures was found to be up to five times higher than brine alone but the microstructure was easily destroyed, and not readily regained, under high shear conditions. At higher temperatures and higher ionic strength, the effect is less pronounced. These results were considered in the context of flow through porous media, and the effect on buoyancy-driven flow is significant. Understanding this effect is important for developing an accurate constitutive relationship for leaking $CO_2$, which will lead to better capacity to select and monitor GCS sites.

**Citation:** Wang, S., and A. F. Clarens (2012), The effects of $CO_2$-brine rheology on leakage processes in geologic carbon sequestration, *Water Resour. Res.*, *48*, W08518, doi:10.1029/2011WR011220.

## 1. Introduction

[2] Geologic carbon sequestration (GCS) is a promising approach for addressing the medium-term goal of providing carbon-neutral energy while utilizing existing fossil fuel-based infrastructure [*Bachu and Adams*, 2003; *Eccles et al.*, 2009]. In GCS, flue gas is captured from point sources, such as power plants, and the $CO_2$ is separated, compressed, and injected into porous geologic formations where the $CO_2$ will exist in the liquid or supercritical phase due to the large hydrostatic pressures and geothermal temperatures in the formation [*Chen and Zhang*, 2010; *Yang and Gu*, 2006]. The density of $CO_2$ under these conditions is lower than the density of the connate brines, and so a bubble of $CO_2$ will be subject to upward buoyant forces. Host formations must be bound by an impermeable caprock to prevent the buoyant forces from allowing rapid leakage of the $CO_2$ to the atmosphere [*Kneafsey and Pruess*, 2010; *Lackner*, 2003]. A large body of academic and industrial work suggests that GCS could be one of the most effective means to prevent many gigatons of carbon from entering the atmosphere over the next several decades [*Benson and Cole*, 2008; *Dooley et al.*, 2006; *Gasda et al.*, 2011; *IPCC*, 2005].

[3] The benefits of GCS would be diminished if $CO_2$ leaked to the atmosphere in appreciable amounts. Overcoming capillary and chemical barriers, $CO_2$ could escape from host formations through heterogeneities in caprocks, faults, or improperly plugged abandoned wells [*Nordbotten et al.*, 2005; *Wollenweber et al.*, 2010; *Zhang et al.*, 2009]. Leakage would not only represent a loss of carbon mitigation credits, it could also cause a net contribution to greenhouse gas emissions because of the energy consumed in the failed $CO_2$ capture and storage operation [*Pollak and Wilson*, 2009]. Leakage may also have environmental consequences, such as contamination of water resources or, worse, dangerous displacement of oxygen at the land surface [*Birkholzer and Zhou*, 2009]. Eruptions from naturally occurring reservoirs provide evidence for the possibility of discharges of $CO_2$ from the subsurface [*Pruess*, 2008b]. These processes are difficult to study at the field scale because of the extensive heterogeneity that exists at these sites and because cause-and-effect relationships are difficult to establish [*Oldenburg et al.*, 2010; *Patzek et al.*, 2003].

[4] The fundamental processes driving $CO_2$ leakage from deep subsurface porous formations are poorly understood [*Oldenburg and Lewicki*, 2006]. Figure 1 illustrates how the phase behavior of $CO_2$ is influenced by depth and the natural geothermal gradients that exist in the subsurface. For $CO_2$

[1]Department of Civil and Environmental Engineering, University of Virginia, Charlottesville, Virginia, USA.

Corresponding author: A. F. Clarens, University of Virginia, 351 McCormick Rd., Thornton Hall, Charlottesville, VA 22904, USA. (aclarens@virginia.edu)


0043-1397/12/2011WR011220

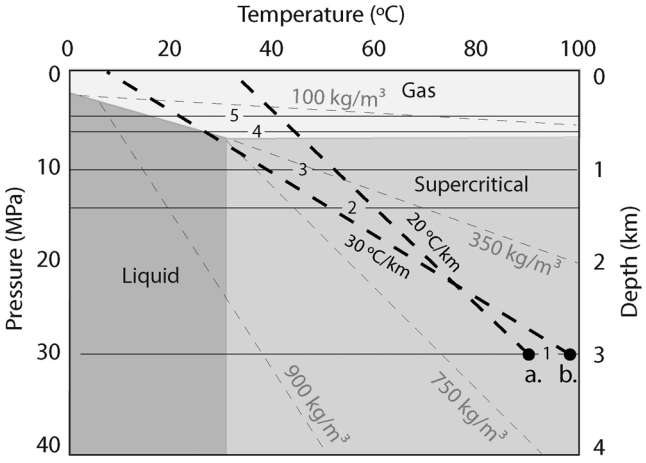


**Figure 1.** Phase behavior of $CO_2$ in the subsurface is a function of the depth, surface temperature and the thermal gradient in the subsurface. Letters a. and b. correspond to two possible leakage pathways for $CO_2$ that would have implications for the phase behavior and density conditions. The horizontal numbered lines correspond to the conditions listed in Table 1 that illustrate how $CO_2$ density/phase behavior will impact leakage.

injected at similar depths at different sites, indicated with dashed lines a and b in Figure 1 (the black circles represent the $CO_2$ reservoirs), the buoyant forces on a rising bubble of $CO_2$ may grow due to the increased buoyancy that comes from expansion of $CO_2$ from supercritical (i.e., $CO_{2(sc)}$) to subcritical conditions (i.e., either $CO_{2(l)}$ or $CO_{2(g)}$) [*Oldenburg*, 2007; *Pruess*, 2008b]. The relationship between density and phase behavior at the five depths indicated using the horizontal lines in Figure 1 are further described in Table 1. As the $CO_2$ moves toward the surface and becomes gas, the density decreases appreciably and the buoyant driving force on $CO_2$ keeps growing during the entire process. The density data presented here show how the phase characteristics of $CO_2$ could result in nonlinear differences between the density of the brine and the $CO_2$. In some cases (as in path a), the $CO_2$ will transition directly from supercritical to gas phase resulting in a drop in density, while in others (as in path b) the density of the fluid will increase as it transitions from supercritical to liquid phase, followed by a sharp decrease as it transitions to gas. Density is not the only characteristic that matters in understanding leakage rates; permeability and capillarity associated with the porous media, which are site specific, will play a major role. In addition, if the bubble rises quickly, adiabatic expansion and associated Joule-Thomson cooling would tend to mitigate the density difference [*Pruess*, 2008a]. The viscosity contrast between a rising bubble of $CO_2$ and the brine it is displacing increases, making it more likely to develop instabilities and fingering [*Riaz and Tchelepi*, 2008].

**Table 2.** The Shear Experienced by Rising Bubbles of $CO_2$ in the Subsurface is Strongly Influenced by the Bubble Velocity and Geometry of the Pores Through Which It Is Flowing

| | Shear Rate ($s^{-1}$) | |
|---|---|---|
| Diameter (m) $\times 10^{-5}$ | Velocity = 0.001 (m/s) | Velocity = 0.002 (m/s) |
| 2 | 200 | 4000 |
| 4 | 50 | 1000 |
| 6 | 33 | 666 |
| 8 | 25 | 500 |
| 10 | 20 | 400 |

[5] Ultimately, leakage will be influenced by many factors other than density, such as formation permeability or capillarity. To understand this complex behavior, it is useful to consider the case of discrete $CO_2$ bubbles, where rise can be understood in terms of a force balance that impacts capillary trapping and dissolution/precipitation reactions [*Li et al.*, 2006]. The dynamic forces acting on the bubble of $CO_2$ are generally thought to fall into one of three categories: (1) buoyant forces; (2) interfacial tension forces; and (3) shear drag forces [*Corapcioglu et al.*, 2004; *Oldenburg and Lewicki*, 2006]. Of these, the viscous shear forces in the brine, which is directly affected by viscosity, will have an appreciable but poorly understood impact on the transport of buoyant $CO_2$. The shear experienced by a rising bubble of $CO_2$ through porous media can be quite high. Table 2 provides estimates of the shear rate that would be expected on a rising $CO_2$ bubble through porous media using representative pore sizes and flow velocities [*Juanes et al.*, 2006].

[6] Most of the work to date on $CO_2$-brine mixtures has been carried out for FLE mixtures (defined in Figure 4) at high pressure (≥10 MPa) and low shear conditions (<10 $s^{-1}$) [*Bando et al.*, 2004; *Kumagai and Yokoyama*, 1999]. These studies rely on falling capillary tube or solid particle viscometers where shear cannot be independently controlled and cannot be used to study non-Newtonian behavior [*Bando et al.*, 2004; *Kumagai and Yokoyama*, 1998; *Silin et al.*, 2009]. Geologists studying the flow of magma in the subsurface have recognized that the presence of multiple phases can result in complex non-Newtonian flow behavior [*Llewellin et al.*, 2002b; *Manga and Loewenberg*, 2001]. The estimates presented in Table 2 suggest that $CO_2$-brine

**Table 1.** Representative Temperature Pressure Conditions for Leaking $CO_2$ Under Two Geothermal Gradients[a]

| | | | Leakage Pathway a ($T = 30 + 20D$) | | | | Leakage Pathway b ($T = 5 + 30D$) | | | |
|---|---|---|---|---|---|---|---|---|---|---|
| Number | Pressure (MPa) | Depth (km) | Temperature (°C) | Density (kg/m³) | Phase | Δ Specific Weight (N/m³) | Temperature (°C) | Density (kg/m³) | Phase | Δ Specific Weight (N/m³) |
| 1 | 30 | 3 | 90 | 703.27 | SC | 973.0 | 95 | 682.39 | SC | −170.3 |
| 2 | 15 | 1.5 | 60 | 604.09 | SC | 2155.8 | 50 | 699.75 | SC | −128.1 |
| 3 | 10 | 1 | 50 | 384.33 | SC | 1947.4 | 35 | 712.81 | SC | −116.6 |
| 4 | 7 | 0.7 | 44 | 185.81 | V | 713.7 | 26 | 724.7 | L | 5729.5 |
| 5 | 5 | 0.5 | 40 | 113.05 | V | | 20 | 140.65 | V | |

[a]Nonlinear differences in density driven by the $CO_2$ phase characteristics in pathways a and b could result in complex flow behavior (as illustrated by the Δ Specific Weight term). The numbers in the first column correspond to the depths presented in Figure 1. Phase definitions are as follows: SC = supercritical, L = liquid, V = vapor, D = Depth and T = Temperature.

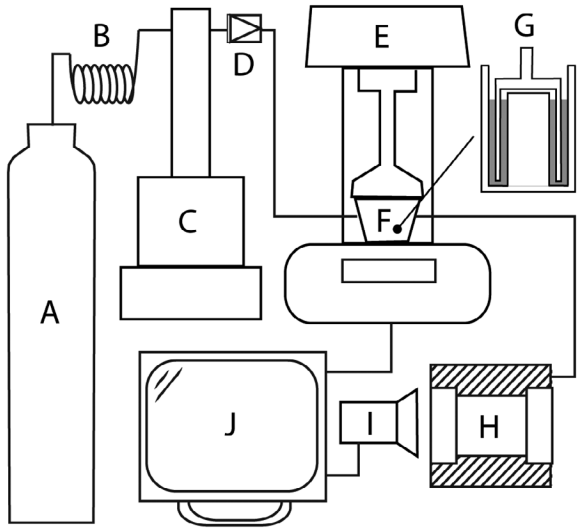


**Figure 2.** Schematic of experimental setup. A is the tank of food-grade $CO_2$, B is the heat exchanger, C is the syringe pump, D is the check valve, E is the rotational rheometer, F is the high-pressure cell, G is the double-gap attachment, H is the high-pressure view cell, I is the digital camera, and J is the computer.

mixtures may experience shear on the order of 20–4000 $s^{-1}$, and so complex flow behavior is possible. The nonlinear rheological behavior of multiphase $CO_2$-brine mixtures has been reported in terms of interfacial behavior but not explored in detail for the bulk of the $CO_2$-brine mixture [*Kloek et al.*, 2001; *Tewes and Boury*, 2005].

[7] Understanding the flow of two-phase mixtures in porous media is vital for understanding trapping and leakage processes in the context of GCS. At present, our understanding derives from theoretical simulations that predict outcomes ranging from self-enhancing flow to self-limiting flow [*Pruess*, 2008b; *Silin et al.*, 2009]. To fill the gap in understanding whether $CO_2$-brine rheology will enhance or suppress leakage, this work explores the viscosity of single and multiphase $CO_2$-brine mixtures under a range of GCS-relevant conditions. The experiments were focused on the laminar conditions, which would likely prevail during a gradual leakage process. These experimental results are then considered in the context of existing modeling frameworks that help evaluate the significance of the findings.

## 2. Experimental Methods

[8] The rheological properties of $CO_2$-brine mixtures were characterized using an Anton-Paar® Physica MCR 301 rotational rheometer. The rheometer allowed for the measurement of viscosity values over a broad range of temperature, pressure, and shear conditions. The rheometer was equipped with two interchangeable high-pressure cells rated up to 15 MPa with precise (±0.1°C) peltier-style temperature control. Two cells of different size were used to measure low (<100 $s^{-1}$) and high (>100 $s^{-1}$) shear rates. Both cells were equipped with double-gap measuring geometries especially designed for low-viscosity measurements. Since the effective shear measured by the rheometer is perpendicular to the circumference of the measuring tool, but not to the fluid, the shear force can be decomposed into a normal force and an axial extensional force [*Djéridi et al.*, 1999]. This effect has been reported for study of bubbly flow in the past and is especially relevant for understanding how bubbles will flow through porous media where bubbles will experience shear and extensional forces from the pore walls and pore throats [*Nakken et al.*, 2001; *Thompson et al.*, 2001]. In addition, the gap in the measurement tool is on the same order of magnitude of the pores that would exist in sequestration sites to capture scale-dependent effect on bubble deformation. The $CO_2$-brine mixtures were prepared using a Teledyne ISCO 500HP high-pressure syringe pump with a constant temperature jacket. The $CO_2$ was delivered as received (Roberts Oxygen Co., Charlottesville, VA). The brine was made using analytical-grade sodium chloride (Fisher Scientific, Hanover Park, IL) and was used as delivered. The pressure cell was also attached to a custom-built high-pressure view cell to enable real-time recording and visualization of the phase behavior of the $CO_2$-brine mixture using a CCD firewire camera. A schematic of the experimental setup is presented in Figure 2.

[9] The experimental setup employed here was found to produce accurate results for shear rates ranging from 40 to 1000 $s^{-1}$. The transition between laminar and turbulent flow was found to occur around a shear rate of 1100 $s^{-1}$ by experimental trials and calculations based on published protocol [*Nakken et al.*, 2001]. No measurements were made above this value. To eliminate the possibility that dissolved air could interfere with the measurements, water was boiled prior to use in the experiments. In addition, the components of the pressure cell were prewetted and allowed to equilibrate with the sample to minimize interference from entrained air. All samples were given adequate time, usually on the order of several hours, to reach equilibrium of saturation before running an experiment. The exact composition of the $CO_2$-brine solutions was calculated using the method described by Bando *et al.* [*Bando et al.*, 2003] and using the solubility relationship shown in Figure 3. Under both fluid

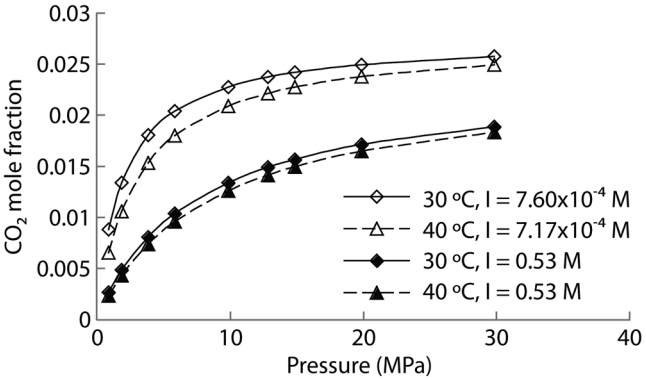


**Figure 3.** Solubility of $CO_2$-brine mixtures was controlled to produce conditions that were representative for a rising bubble of $CO_2$ along its path toward the surface. All of the results in this study were conducted for pressures at or below 10 MPa, since this is the range most relevant for leakage processes and the least characterized in the existing literature. All experimental methods were also benchmarked using deionized water to ensure that the methods produced the expected behavior and to produce a comparison with the $CO_2$-brine systems.

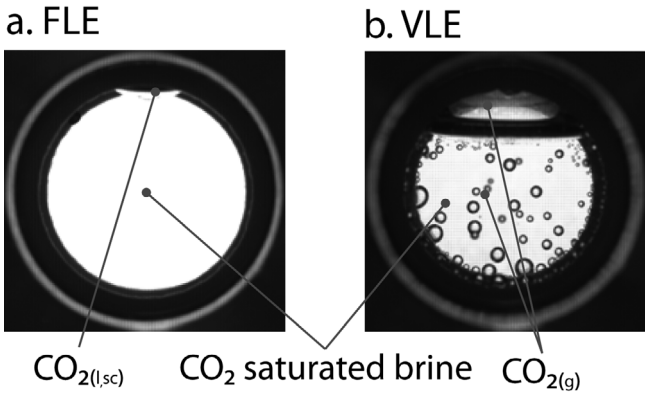


**Figure 4.** The experimental work presented here focused on (a) $CO_2$-saturated brines under FLE conditions and (b) $CO_2$-brine suspension under VLE conditions. Here, images of these two conditions are provided as seen through the high-pressure view cell connected to the rheometer.

liquid equilibrium (FLE) and vapor liquid equilibrium (VLE) conditions (Figure 4), these curves were used to identify both the composition of the mixture and the pressure at which phase separation would occur.

[10] The mixtures under FLE equilibrium were made by pressurizing the high-pressure vessel in the rheometer and adding $CO_2$ to achieve the desired conditions. To create VLE conditions, saturated $CO_2$-brine mixtures under FLE conditions were gradually depressurized to create multiple-phased $CO_2$ bubbly suspension. Figure 3 illustrates how a small change in pressure can elicit a significant change in solution chemistry, particularly at the low-pressure ranges that were the focus of this work. Figure 4 provides a visual example of the distinction in phase behavior between FLE and VLE conditions in the context of $CO_2$-brine flow through the subsurface. Upon depressurization, liquid or supercritical $CO_2$ will maintain a distinct meniscus with water that minimizes surface area as seen in Figure 4a. As the $CO_2$ transitions to gas phase, bubbles will form as seen in Figure 4b. This creation of an immiscible new phase can be understood in terms of the solubility of $CO_2$ in water and the thermodynamics that govern the formation of this new phase. As seen in Figure 3, the derivative of the solubility of $CO_2$ in water is much greater at lower pressures. A fixed drop in pressure will result in much more phase separation when in the gas phase versus the liquid or supercritical phase [*Oldenburg and Lewicki*, 2006]. This behavior can also be explained in terms of the thermodynamics of bubble formation according to the Kelvin equation [*Adamson*, 1997]. The accretion of $CO_2$ is unfavorable for the liquid or supercritical $CO_2$ by virtue of their lower interfacial tension with brine and greater energy barrier. During the experiments, a stir bar was placed inside the view chamber and the shear conditions were set to match those in the rheometer pressure cell. With the stir bar spinning, reorientation, rearrangement, and deformation of bubbles did occur. Under the experimental shear conditions, no significant inter-bubble interactions such as collision or nucleation of bubbles were observed under laminar condition, so the modeling efforts focus on bubble-liquid interactions and neglect bubble-bubble interactions. Within the shear rate range studied here, no wall slip of $CO_2$ bubbles on the inner surface of the pressure view cell was observed. In addition, no significant normal stress difference or stress relaxation was detected.

## 3. Results and Discussion

[11] In subsurface formations that are suitable for GCS, the hydrostatic pressure near the injection well keeps the $CO_2$ in the liquid or supercritical phase. Under the resulting FLE conditions, the $CO_2$-brine mixtures exhibit Newtonian behavior and the presence of $CO_{2(aq)}$ increases the viscosity of mixture as shown in Figure 5. The magnitude of the viscosity increase is generally proportional to the $CO_{2(aq)}$ concentration in the solution. This effect has been reported before [*Bando et al.*, 2004; *Kumagai and Yokoyama*, 1999] and is consistent with the behavior of other acid solutions [*Laliberté*, 2007]. The results presented in Figure 5 are for a lower pressure or $CO_2$ mole fraction ($\chi_{CO_2}$) range than has appeared in the literature to date. Since $CO_2$ mole fraction is controlled by the partial pressure of $CO_2$ in equilibrium with the aqueous phase, the $x$ axis in Figure 5 could be expressed using the relationship in Figure 3. This range was selected specifically to enable better understanding of leakage processes from geologic sequestration sites. Interestingly, the results reveal a subtle dip in the values near the pressure that $CO_2$ transitions from liquid/supercritical fluid to gas (around a $CO_2$ mole fraction of 0.01). This effect can be understood in light of two competing mechanisms that drive the viscosity of the FLE mixture. The first is associated with the acidification of the brine solution resulting from the dissolution of $CO_2$ in the mixture and the formation of carbonic acid, represented by the top line in Figure 6. Aqueous acid solutions have higher viscosity than water on account of the more intimate molecular interactions between conjugate species [*Kumar et al.*, 2009; *Laliberté*, 2007; *Zafarani-Moattar and Majdan-Cegincara*, 2009]. The second effect produces a decrease in the viscosity of the brine as a result of

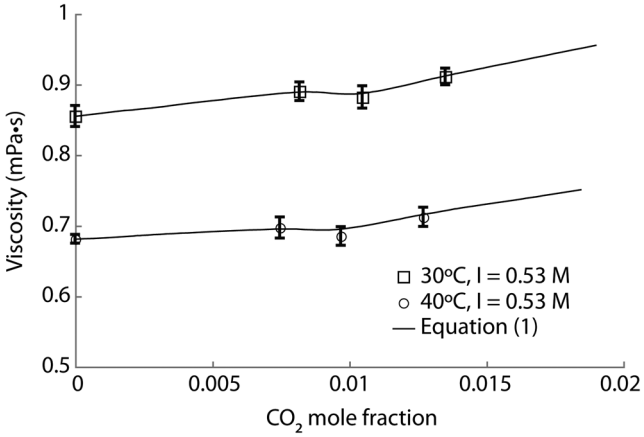


**Figure 5.** The viscosity of $CO_2$-brine mixtures under FLE conditions increases with $CO_2$ concentration as shown in other work, but the results here, for a lower equilibrium concentration of $CO_2$, show a dip around the point that $CO_2$ transitions from liquid (30°C)/supercritical (40°C) to gas. The four data points on each line correspond to experimental conditions of 0.1, 4, 6, and 10 MPa from left to right. These data are for I = 0.53 M, but the same trend was observed at lower ionic strength values. Error bars represent 90% confidence interval.

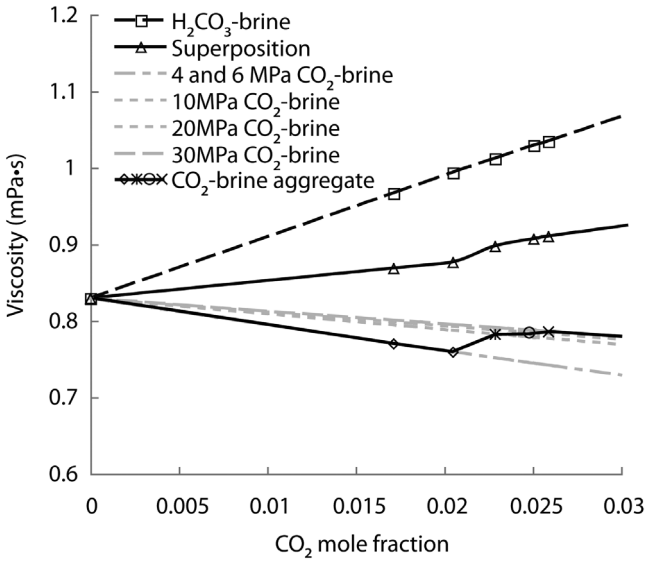


**Figure 6.** The Grunberg-Nissan model accurately captures the viscosity of FLE mixtures. The viscosity of $CO_2$-brine solutions generally increases with $CO_2$ concentration even though there is a minor drop in viscosity near the point where $CO_2$ transitions from liquid/supercritical to gas.

mixing a lower viscosity fluid, in this case $CO_2$ with the brine, represented by the bottom group of lines in Figure 6. The latter effect is less significant so that the net effect of $CO_2$ on the brine is to increase the viscosity, though the importance of both mechanisms is evident near the vapor/liquid transition point.

[12] The competing mechanisms that influence the viscosity of $CO_2$-brine mixtures under FLE conditions can be understood in the context of Arrhenius type mixing rules. This type of model suggests that the viscosity of a binary mixture will be proportional to the relative composition (in this case, $\chi_{brine}$ and $\chi_{CO_2}$) and the viscosity ($\mu_{brine}$ and $\mu_{CO_2}$) of those two fluids. The Grunberg-Nissan equation, which is based on Arrhenius-type behavior but also includes an interaction parameter for the species in solution, accurately predicts the behavior of these mixtures [*Kijevčanin et al.*, 2008; *Laliberté*, 2007; *Soli and Byrne*, 2002; *Tomida et al.*, 2007]. In this case, the interaction term accounts for the increase in viscosity that is associated with adding a weak acid to the solution:

$$\ln \mu_{m,FLE} = \chi_{CO_2} \ln \mu_{CO_2} + \chi_{brine} \ln \mu_{brine} + \frac{1}{2} \chi_{CO_2} \chi_{brine} \cdot \left( G_{CO_2-brine} + G_{brine-CO_2} \right) \quad (1)$$

where $\mu_{m,FLE}$ is the viscosity of the mixture under FLE conditions and $\mu_i$ and $x_i$ are the viscosity and the mole fraction of species $i$, respectively. $G$ is the interaction coefficient of components. In the case of FLE $CO_2$-brine homogenous mixtures, the Grunberg-Nissan equation does a good job of approximating the experimental results of Figure 5. In particular, at the transition from liquid/supercritical to gaseous $CO_2$, the $\mu_{CO_2}$ changes substantially. The net effect on the viscosity of the solution is the dip near the transition pressure. Experimental data of pure substances including brine and $CO_2$ were used, and a graphical representation of this effect at 30°C is provided in Figure 6. The top line provides an estimate of how the viscosity of a FLE $CO_2$-brine mixture should look according to the Grunberg-Nissan equation if carbonic acid only resulted in producing a higher viscosity solution like other acids. The bottom grouping of lines shows how the viscosity of a $CO_2$-brine solution might be interpreted if $CO_2$ only had the effect of reducing the viscosity of the mixture, since the viscosity of the $CO_2$ is always lower than the brine. Several lines are used since the properties of $CO_2$ change as a function of equilibrium pressure, and that is proportional to the composition plotted on the $x$ axis. For a range of $\chi_{CO_2}$, the model accurately captures the viscosity behavior of the mixture, including the dip in viscosity near the pressure at which $CO_2$ transitions from liquid/supercritical to gas phase.

[13] In the broader context of predicting leakage from geologic sequestration sites, the dip in solution viscosity observed under the FLE condition will likely have only a small effect on bubble rise. The effect that temperature and ionic strength play in driving the viscosity of the brine solutions, both in terms of the viscosity of the water and in limiting the solubility of $CO_2$, is much more pronounced than the dip that occurs near the transition from liquid/supercritical to gas phase $CO_2$. Additional tests, i.e., shear sweep, transient, and hysteretic tests, reveal that FLE mixtures are Newtonian under variable shear conditions or over time, with the shear sweep results shown in Figure 7. This is expected since both brine and $CO_{2(g,l,sc)}$ are Newtonian fluids. The results are highly consistent with published data for low shear conditions providing a useful benchmark for the experimental techniques used here [*Bando et al.*, 2004].

[14] As $CO_2$ or $CO_2$-saturated brine moves to shallower depths, the pressure of the surrounding formation will decrease and $CO_2$ will undergo a phase transition to create VLE conditions. The results of experiments under VLE conditions were found to be somewhat more complex because of the presence of viscoelastic $CO_2$ bubbles.

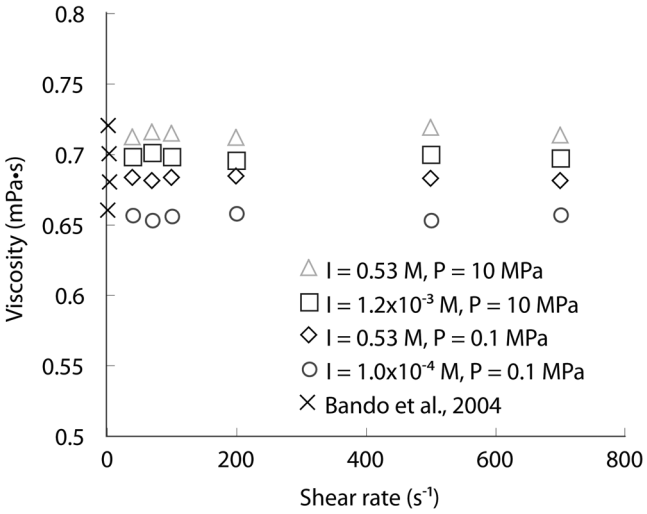


**Figure 7.** Under FLE conditions, $CO_2$-brine solutions exhibit Newtonian behavior over a wide range of shear rates. The data presented here were collected at 40°C, but the trend is consistent at 30°C.

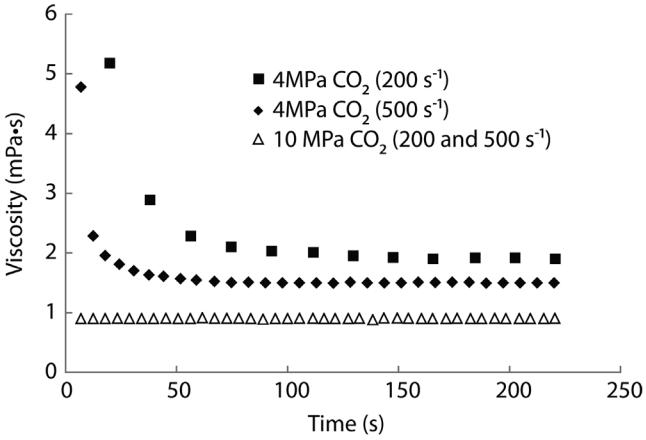


**Figure 8.** The viscosity of $CO_2$-brine mixtures under VLE conditions at 30°C, I = 0.53 M, and two shear rates (shaded markers) reveals that complex flow behavior can be expected once $CO_{2(g)}$ bubbles appear in the brine, resulting in different steady state effective viscosities for the mixture. FLE results are represented using markers with no fill.

Extensive work in volcanology has demonstrated how magma flows with entrained gas bubbles exhibit non-Newtonian flow behavior [*Manga and Loewenberg*, 2001]. This behavior is driven indirectly by mixture composition and state variables like temperature and pressure and more directly by bubble volume and size distribution, shear rate, and time [*Llewellin and Manga*, 2005]. There are differences between magma and brine in terms of viscosity, interaction with gases, and shear conditions that require separate analysis. A series of shear sweep, transient, and thixotropic tests was designed to understand the effect that $CO_2$ bubbles will have on brine flows under VLE conditions.

[15] Studies of the VLE flow conditions in the $CO_2$-brine system confirmed that there was a nonlinear relationship between shear stress and shear rate. The results of Figure 8 demonstrate that under lower pressure conditions (≤4 MPa) where VLE occurs, the mixture exhibits time-dependent behavior. The effective viscosity of the mixture is initially quite high, but it decreases readily under applied shear toward a steady state that is higher than the viscosity of the brine alone. After tens of seconds under applied shear, the effective viscosity of the solution approaches the steady state value. To explain this, it is helpful to envision how a single $CO_{2(g)}$ bubble might resist deformation at the beginning of the experiment while its shape is changed from spherical to elliptical. The viscoelastic behavior that is observed in the bulk fluid is the result of many bubbles of different sizes exhibiting resistance to applied shear stress and the corresponding increase in the gas-liquid interfacial area and energy per unit volume [*Klempner and Frisch*, 1991]. Steady state conditions are characterized by equilibrium between the interfacial tension force and shear stress. Interestingly, the steady state viscosity of the VLE mixture is always higher than that of the FLE conditions. This is significant because it suggests that even over long time periods, the presence of $CO_{2(g)}$ bubbles could suppress leakage relative to brine with $CO_{2(aq)}$ dissolved in it. The results of Figure 8 also suggest that at lower shear rates, the steady state viscosity of the VLE mixture is higher. This is because at lower shear, the shearing energy acting to deform the bubbles is lower, and so the streamline deformation effect caused by $CO_{2(g)}$ in the solution is more pronounced, causing a higher effective viscosity for the mixture. In other words, the larger the shear forces placed on the bubbly $CO_2$-brine suspension, the closer it approximates the viscosity of a $CO_2$-brine solution under comparable FLE conditions.

[16] The effect of entrained bubbles on fluid flow has been explored in great detail for a number of other systems [*Llewellin et al.*, 2002a]. The literature suggests that under certain conditions, the presence of bubbles can either increase or decrease the viscosity of the mixture relative to the continuous phase. The increase is typically associated with streamline distortion as viscoelastic bubbles interfere with fluid flow. An initial input of energy is needed during the evolution of the bubbles from solid-like to liquid-like (elastic to viscous) structures, which results in an apparent shear-thinning behavior as seen in Figure 8. Decreases in mixture viscosity are typically associated with free slip of matrix fluid along the highly deformed bubble surface. Even though preliminary experiments suggested that $CO_2$-brine mixtures would typically fall into the former category, it was worth exploring the exact conditions that led to this behavior.

[17] Constitutive relationships of multiphase flow are typically based on the derivation of a relative viscosity term, $\eta_r$, which is defined as the ratio of the viscosity of the suspension normalized to the suspending matrix fluid. The relative viscosity of a bubbly mixture can generally be expressed as a function of several properties that can be measured in the laboratory, including the volumetric fraction of $CO_{2(g)}$ bubbles ($\phi$), the size distribution of $CO_{2(g)}$ bubbles ($R_i$, the radius of the $i$th group of bubbles with identical size), the viscosity of the continuous phase ($\mu_0$) and capillary number ($C_a$), a dimensionless number that captures the ratio of viscous shear force to interfacial tension force [*Llewellin and Manga*, 2005] given by

$$C_a = t_r \dot{\gamma} \tag{2}$$

where $\dot{\gamma}$ is the shear rate and $t_r$ is the bubble relaxation time, which is a measure of the time scale over which a bubble can respond to changes in its shear environment [*Llewellin and Manga*, 2005]. The $t_r$ is a weakly increasing function of $\phi$ and is expressed as $t_r = \frac{\mu_0 a}{\sigma}$, where $a$ is the radius of the undeformed $CO_{2(g)}$ bubble and $\sigma$ is the interfacial tension between $CO_{2(g)}$ bubble and brine [*Llewellin and Manga*, 2005]. For unsteady flows, where the rate of change of the shear strain rate, $\ddot{\gamma}$, must be considered, it is common to use the dynamic capillary number, given by

$$C_d = t_r \frac{\ddot{\gamma}}{\dot{\gamma}} \tag{3}$$

For the $CO_2$-brine mixtures considered here, $t_r$ was found to be $3.3 \times 10^{-6} \sim 1.0 \times 10^{-4}$ s using published interfacial tension values [*Bachu and Brant Bennion*, 2009]. The $\phi$ and $R_i$ were 0.5–4 vol% and $2.0 \times 10^{-4} \sim 5.0 \times 10^{-3}$ m, respectively. $C_a$ was used for the steady state experiments (i.e., Figures 8–10) and $C_d$ for the unsteady flow experiments (i.e., Figures 11 and 12), and they were found to be $6.7 \times 10^{-4} \sim 1.0 \times 10^{-1}$ and $8.3 \times 10^{-8} \sim 5.0 \times 10^{-3}$, respectively.

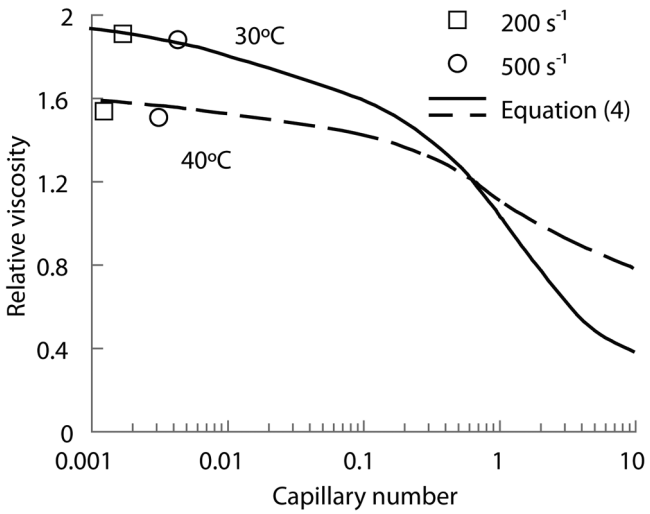


**Figure 9.** The steady state relative viscosity of VLE $CO_2$-brine suspensions will always be higher than the viscosity of the suspending matrix fluid, pure brine saturated with $CO_2$. This has important implications for multiphase flow in leakage situations related to carbon sequestration. Experimental results presented here are at 2 MPa and I = 0.53 M.

[18] A number of semiempirical relationships between $C_a$ or $C_d$, $\phi$, and $\eta_r$ have been proposed in previous work [*Llewellin et al.*, 2002a; *Murai and Oiwa*, 2008; *Sochi*, 2010]. Several equations were tested here, and the best fit was obtained using a model that accounts for polydispersity and instability of bubbles called the gamma probability density function, given by

$$\eta_r = \left(1 - \frac{5}{3}\phi\right) + \frac{8}{3}\phi \int_0^\infty \frac{\frac{\beta^\alpha}{\Gamma(\alpha)} R_i^{\alpha-1} e^{-\beta R_i}}{1 + \frac{9}{16}\left(\frac{\mu_0 \dot{\gamma}}{\sigma}\right)^2 R_i^2} dR_i \qquad (4)$$

where $\Gamma(\alpha)$ is the gamma distribution function; $\mu_0$ is the viscosity of the continuous phase; and $\alpha$ and $\beta$ are the shape and scale parameters, respectively, which are obtained by fitting experimental results [*Joh et al.*, 2010]. This model provides accurate approximations of the rheology of bubbly flow for polydispersed bubble suspensions in shear flows over a wide range of capillary numbers [*Joh et al.*, 2010; *Sang-Yoon et al.*, 1997].

[19] The relative viscosity of $CO_2$-brine mixtures under VLE conditions at steady state is presented in Figure 9. Both experimental and modeling results based on equation (4) are presented. The capillary number on the $x$ axis in Figure 9 is calculated based on the weight-averaged $R_i$. The results are consistent with the data presented in Figure 8, where the effective viscosity of the bubbly suspension is higher than the viscosity of the $CO_2$-saturated brine alone (i.e., $\eta_r > 1$). It was determined that $CO_2$-brine suspensions will always increase the viscosity of the solution, and this can be explained using two characteristics of bubbly flow. The first is that brines have a relatively low viscosity and so the capillary number will always be $\ll 1$. As described above, $C_a$ was several orders of magnitude lower than 1, and per bubbly flow rheology, this is the transition point at which streamline deformation becomes less pronounced and shear slip along the bubble brine interface becomes the dominant characteristic of the fluid. The second reason that $CO_2$ bubbles will always increase the viscosity of brines in geologic carbon sequestration conditions is that the flow of interest occurs through porous media and the capillary number in these types of conditions is characteristically low.

[20] It is important to note that most of the work on relative viscosity to date assumes that the liquid/supercritical phase and the gas are immiscible. This is not the case for $CO_2$ in brine since the two are quite miscible and under nonequilibrium conditions, applied shear could accelerate gas exchange with the brine since it would increase the contact area between the two phases. The results of this effort could help inform models in which the $CO_{2(g)}$ is leaking into brine-filled formations for the first time (e.g., in terms of predicting mixing rates and so on) but these were not the conditions assessed here. This work was carried out for the case where the brine is already saturated with $CO_2$

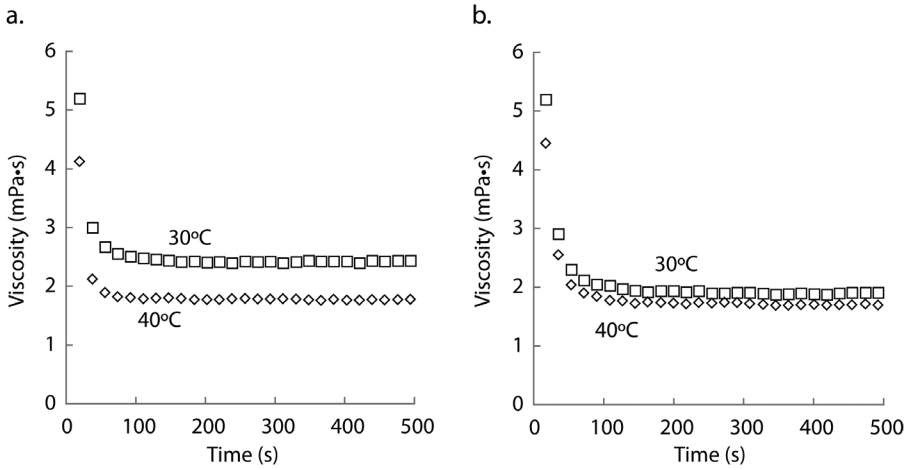


**Figure 10.** The viscosity of $CO_2$-brine mixtures under VLE conditions (4 MPa at the shear rate of 200 $s^{-1}$) at two temperatures (30°C and 40°C) and ionic strength ((a) I = 7.17 – 7.6 × $10^{-4}$ M; (b) I = 0.53 M) conditions. Higher temperature and ionic strength both suppress the formation of $CO_{2(g)}$ bubbles, which result in lower values of steady state viscosity.

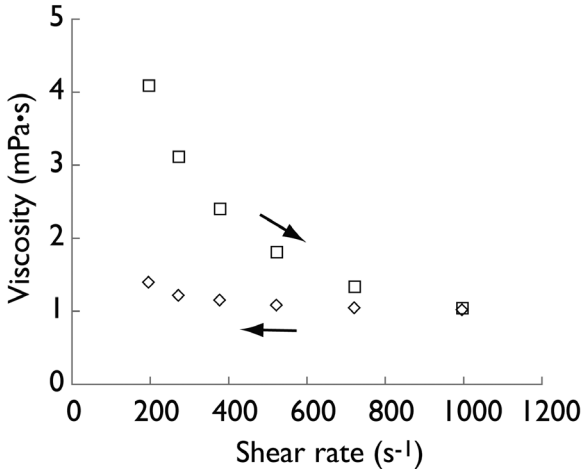


**Figure 11.** Under VLE conditions, $CO_2$-brine mixtures exhibit flow hysteresis whereby the presence of $CO_{2(g)}$ bubbles results in a drop in viscosity as shear is applied to the fluid. This structure is lost permanently as the shear is removed from the fluid. This path dependence has important implications for site selection in GCS (these results are for 30ºC, I - 0.53 M).

under equilibrium conditions. Geologic sequestration sites must be stable over decades and centuries, and so equilibrium conditions are of the greatest interest.

[21] To evaluate the effect that solution chemistry has on the complex flow of $CO_2$-brine suspensions under VLE conditions, the rheology of the system was measured under two ionic strength conditions, ~0 and 0.53 M. The results, presented in Figures 10a and 10b, respectively, suggest that ionic strength has a net effect of decreasing the effective viscosity of the suspension. This is because the presence of salts in the solution suppresses the formation of $CO_2$ bubbles. Interestingly, ionic strength had the opposite effect on effective viscosity under FLE conditions because the presence of salts in the brine lowered the solubility of $CO_2$ in solution as shown in Figures 3 and 7. From a practical perspective, this suggests that the complex flow behavior can be expected deeper in the subsurface in less saline formations. These results also highlight the strong temperature dependence that is observed in these systems. Since fewer $CO_2$ bubbles form at higher temperatures, the result is a lower effective viscosity for the suspension. The importance of ionic strength is less pronounced at higher temperatures. For both temperatures, the VLE viscosity is substantially higher than it would be under FLE conditions for the same pressure, i.e., comparing the results of Figures 5, 7, and 10.

[22] Another important characteristic of the $CO_2$-brine mixtures under VLE conditions is that the viscosity of the original mixture is not readily regained once the shear forces are removed. This makes sense intuitively because $CO_{2(g)}$ bubbles will become distorted or destroyed in the solution under the applied shear. To measure this behavior in the laboratory, a series of experiments was performed in which the shear on a sample was steadily increased from 200 to 1000 $s^{-1}$, followed immediately by a decrease in the shear rate back to 200 $s^{-1}$. Both the increase and the decrease occurred at the same rate. No rest period was allowed between the two tests. The general trend of these shear sweep tests is illustrated in Figure 11. It is clear that as the shear rate increases, there is a significant drop in viscosity, but that as shear rate is decreased, the mixture viscosity only recuperates to a fraction of its original value. These two

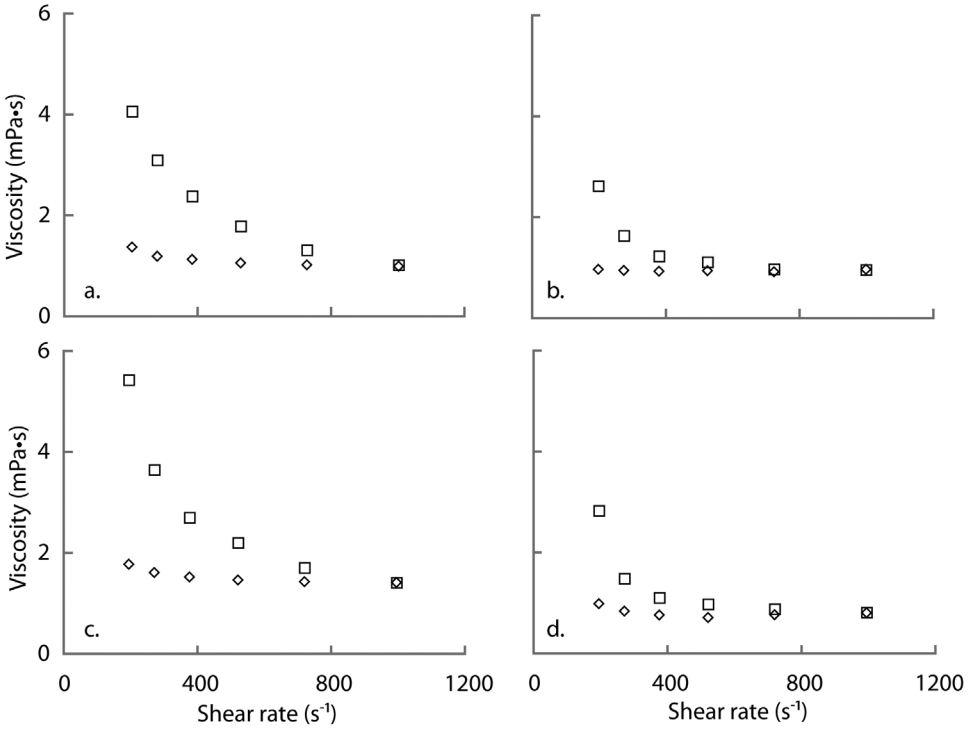


**Figure 12.** Both temperature and ionic strength reduce the magnitude of the thixotropic behavior that was observed under VLE conditions. (a) 30°C, I = 0.53 M; (b) 40°C, I = 0.53 M; (c) 30°C, I = 3.1 × $10^{-4}$ M; (d) 40°C, I = 3.7 × $10^{-4}$ M. All experiments were conducted at 1 MPa.

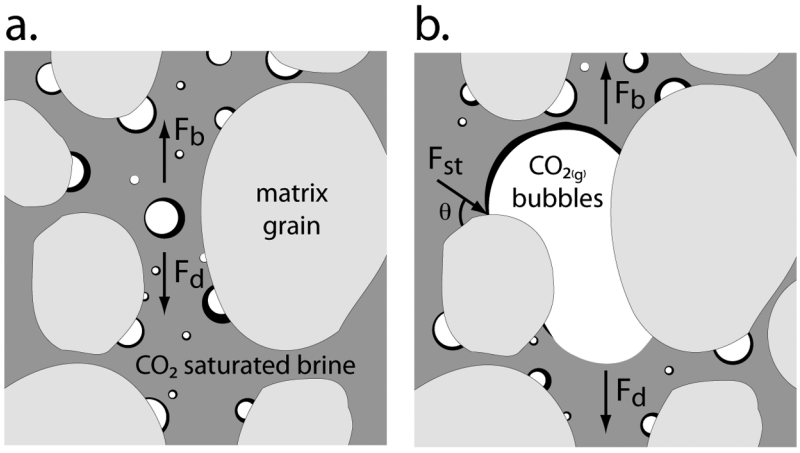


**Figure 13.** Force balance on bubbles of $CO_2$ rising through porous media when (a) $R_{CO_2} < R_P$ and (b) $R_{CO_2} \geq R_P$. Buoyant forces $F_b$ and drag forces $F_d$ act under both scenarios, whereas interfacial tension forces $F_{st}$ act only on those bubbles that contact the pore walls.

curves constitute a so-called hysteresis loop, which is an important characteristic of viscoelastic mixtures. This behavior is most often observed in gels and other complex fluids where hydrogen or ionic bonds result in microstructuring of the fluid [*Barnes*, 1997]. No yield stress was present under the conditions tested. Here the complex behavior is caused solely by the presence of two phases. As the structural units, $CO_{2(g)}$ bubbles in this case, are deformed, there is elongation, rearrangement, and breakdown of bubbles from larger to smaller size and from polydisperse to an increasingly monodisperse distribution.

[23] Consistent with the other experiments reported here, the path dependence of the $CO_2$-brine suspensions when subjected to shear forces is strongly dependent on the pressure, temperature, and ionic strength of the mixture. The shape, height, and area of the hysteresis-loop in Figures 11 and 12 depend on the period and rate of change of shear along with the past kinematic history of the suspension [*Chhabra and Richardson.*, 2008]. The area is related to the energy that is needed to break down the thixotropic structure of the suspension. The size and number of bubbles in the different solutions is a function of ionic strength and the state variables, and so it follows that the energy embodied in the mixtures is different, as shown in Figure 12. Temperature was found to have the most significant impact as shown in Figures 12a and 12b as well as in Figures 12c and 12d. The effect of ionic strength was more modest as seen in Figures 12a and 12c as well as in Figures 12b and 12d. This behavior was tested for several pressures, and the trends were highly consistent for all pressures where VLE conditions exist.

## 4. Effects on Flow Through Porous Media

[24] The results of these experiments will impact bubbly flow of $CO_2$ through porous media in general by slowing the rate of leakage. As leaked $CO_2$-saturated brine moves closer to the surface, the solubility will drop, resulting in the ebullition of small $CO_2$ bubbles. These newly formed bubbles will migrate upwards and expand as pressure declines along the leakage path. Once polydisperse bubbly flow or channel flow ($R_{CO_2} \geq R_P$, where $R_{CO_2}$ is the radius of $CO_2$ bubble and $R_P$ is the equivalent radius of a pore throat in the porous media) conditions ensue, the smaller bubbles may still impact the flow, but the interfacial tension forces and the filtration of bubbles associated with the contact with the geologic formation will come into play. It is important to reiterate that this analysis is for the VLE case in which $CO_2$ exists in the gas phase. The interfacial tension between $CO_2$ and brine or water under high-pressure conditions is too low to support the propagation of small bubbles [*Hebach et al.*, 2002]. At lower pressure (e.g., <5 MPa), the interfacial tension is large enough that we could reasonably assume that small bubbles would form based on the Young-Laplace equation and the Kelvin equation [*Adamson*, 1997]. The pressure inside the $CO_2$ bubble, described by Henry's law must still exceed the sum of the hydrostatic pressure and the interfacial tension between $CO_2$ and brine [*Crandell et al.*, 2010].

[25] When a $CO_2$ bubble is rising freely without contacting the pore wall ($R_{CO_2} < R_P$), vertical transport is driven solely by buoyant forces and retarded by drag forces (Figure 13). For low Reynolds number conditions, the rise velocity of the $CO_2$ bubble can be modeled using Stokes' law [*Poletto and Joseph*, 1995]:

$$u = \frac{{d_{CO_2}}^2 g\left(\rho_{matrix} - \rho_{CO_2}\right)}{\gamma \mu_{matrix}} \tag{5}$$

where $u$ is the rise velocity of $CO_2$ bubble; $d_{CO_2}$ is the diameter of $CO_2$ bubble; $\rho_{matrix}$ and $\rho_{CO_2}$ are the density of the matrix fluid and the $CO_2$, respectively; $\mu_{matrix}$ is viscosity of the matrix fluid; and $\gamma$ is a viscosity coefficient expressed as $\gamma = 12\frac{\mu_{matrix} + 1.5\mu_{CO_2}}{\mu_{matrix} + \mu_{CO_2}}$. Since $\mu_{matrix} \gg \mu_{CO_2}$, $\gamma$ = 12. The Stokes' law is appropriate for small bubbles only because (1) small $CO_2$ bubbles in brine ensure that the Reynolds number is low ($R_e = \frac{\rho_{matrix} u d_{CO_2}}{\mu_{matrix}} \sim 1$) and (2) small $CO_2$ bubbles can be treated as rigid bodies with spherical geometry [*McGinnis et al.*, 2006].

[26] Using the fluid viscosity ($\mu_{matrix}$) results presented in Figures 5 and 7–12, the effects on the Stokes' law estimates of bubble rise velocity can be assessed. The results,

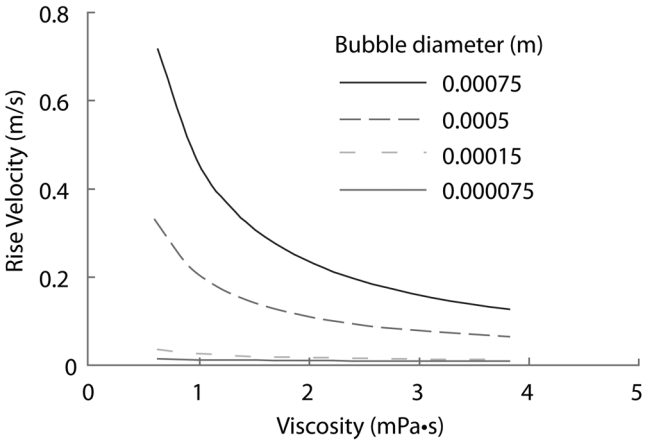


**Figure 14.** Based on Stokes' law, the viscosity of the connate fluid has a dramatic effect on controlling the rise velocity of buoyancy-driven flow of $CO_2$ through brines.

presented in Figure 14, demonstrate that both matrix viscosity and $CO_2$ bubble size affect the rise velocity according to a quadratic proportionality. The viscosity of the brine has an important effect on controlling terminal rise velocity over a range of bubble sizes even though the effect is most pronounced for larger bubbles. This result is worth consideration in light of the viscosity data presented in this work. Once bubble ebullition commences, terminal velocity could drop by more than 75% over a range of relevant bubble sizes. Larger bubbles have a higher terminal velocity, e.g., the terminal velocity of a 0.00075 m bubble is 100 times that of 0.000075 m bubble. The net effect of viscosity and $CO_2$ bubble size on terminal velocity depends on the ratio $\frac{(\Delta d_{CO_2})^2}{\Delta \mu_{matrix}}$. As an example, if a $CO_2$ bubble follows the P-T path described in pathway a in Figure 1, it will have a rise velocity in the range of 0.00085 to 0.643 m/s depending on the salinity of the connate brine. These swings in the rise velocity over orders of magnitude are significant for beginning to bound the uncertainty associated with estimates of $CO_2$ leakage from GCS sites.

[27] For the case in which a $CO_2$ bubble is in contact with the pore walls as channel flow ($R_{CO_2} \geq R_P$) or as polydisperse bubbly flow, the rising bubble will experience interfacial tension force that comes from the ternary contact between the brine, solid, and $CO_2$ in addition to the buoyant and drag forces experienced by a free bubble. Most of the $CO_2$ will flow under this scenario, and so it is of the most interest for understanding how flow through porous media will proceed under these so-called channel flow conditions. The modeling framework used to understand this flow scenario is based on the work of *Corapcioglu et al.* [2004]. The framework is based on a macroscopic force balance and several assumptions: (1) the brine and the $CO_2$ are treated as incompressible; (2) the connate brine is saturated with $CO_2$ such that mass transfer between the bubble and the bulk is not considered; (3) the $CO_2$ is in instantaneous equilibrium with respect to temperature and pressure; (4) the porous media are isotropic and fully saturated with brine before $CO_2$ penetration; (5) there is no bubble generation mechanisms such as snap-off and division; (6) there is no Basset history force that results from the viscous effects generated by the acceleration of a particle relative to a fluid under the creeping flow conditions [*Zhang and Fan*, 2003]; (7) the lift force acting on a bubble is neglected because of irrotational flow conditions [*Soubiran and Sherwood*, 2000]; (8) the fluid flow in the connate brine around a rising bubble and within the fluid bubble is neglected; and (9) velocity gradients are only considered in the vertical direction. This modeling framework has been shown to be a good predictor of bubble rise in unconsolidated media [*Corapcioglu et al.*, 2004].

[28] The governing equation incorporates inertial force, added mass force, buoyant force, interfacial tension force, and drag force that results from the momentum transfer between different phases [*Ergun*, 1952]. Buoyancy force $F_b$ provides the fundamental driver for $CO_2$ to rise, and interfacial tension force $F_{st}$ and drag force $F_d$ resist the motion (Figure 13). The added mass force $F_A$ originates from the acceleration of discrete $CO_2$ mass relative to the matrix fluid in the perturbed flow field [*Wallis*, 1969]. Considering the spatial and transient nature of the rise velocity, linear momentum of $CO_2$ rising in porous media is conserved following equation (6):

$$\sum F = \frac{D}{Dt}\left(\rho_{CO_2} V u\right) = F_A + F_b + F_d + F_{st} = \left(\rho_{CO_2} + C_M \rho_{matrix}\right) V \left(\frac{\partial u}{\partial t} + u\frac{\partial u}{\partial y}\right) \quad (6)$$

where $C_M$ is the added mass coefficient which depends on the geometry of the $CO_2$ bubble, $\rho_{CO_2}$ is the density of $CO_2$, $\rho_{matrix}$ is the density of the matrix fluid, $V$ is the volume of $CO_2$ bubble, and $u$ is the rise velocity of $CO_2$.The added mass term is defined as

$$F_A = \frac{D}{Dt}\left(C_M \rho_{matrix} V u\right) \quad (7)$$

The buoyancy force is defined as

$$F_b = \left(\rho_{matrix} - \rho_{CO_2}\right) g V \quad (8)$$

where $g$ is the acceleration of gravity. The interfacial tension force is

$$F_{st} = 2\pi R_P \sigma \sin\theta \quad (9)$$

where $\sigma$ is the interfacial tension at the $CO_2$-brine interface and can be described with the Young-Laplace equation, and $\theta$ is the equilibrium contact angle of $CO_2$ contacting the wall of the pores. The drag force on the bubble of $CO_2$ is defined as

$$F_d = AV\left[\frac{150\mu_{matrix} u(1-\phi)^2}{d_P^2 \phi^3} + \frac{1.75\rho_{CO_2} u^2 (1-\phi)}{d_P \phi^3}\right] \quad (10)$$

where $A$ is the correction factor incorporating the effects of media-specific properties and contact pattern of $CO_2$ with pore materials such as tortuosity, the shape factor, and surface area [*Cihan and Corapcioglu*, 2008]; $\phi$ is the effective porosity of the porous media; and $d_P$ is the mean diameter of the sedimentary particles. The drag term in this force balance is the most difficult to quantify because the momentum transfer caused by drag force is impacted by heterogeneities in the pore geometry. Recognizing that drag force is associated with both

**Table 3.** Thermophysical Properties Used in Equation (12)

| Parameters | Units | Values | | References |
|---|---|---|---|---|
| Gravitational acceleration, $g$ | m/S$^2$ | 9.81 | | |
| Density of brine, $\rho_{matrix}$ | kg/m$^3$ | 1020 | | [*Duan et al.*, 2006; *Garcia*, 2001] |
| Correction factor, $A$ | | 26.8 | | [*Corapcioglu et al.*, 2004] |
| interfacial tension, $\sigma$ | N·m | 0.04 | | [*Chiquet et al.*, 2007; *Espinoza and Santamarina*, 2010] |
| Contact angle, $\theta$ | Deg | 155.8 | | Experimental data |
| | | Leakage Path a | Leakage Path b | |
| Temperature, $T$ | °C | 40 | 20 | |
| Pressure, $P$ | MPa | 5 | 5 | |
| Density of $CO_2$, $\rho_{CO_2}$ | kg/m$^3$ | 113.05 | 140.65 | [*Span et al.*, 2000] |

viscous and kinetic energy losses, semiempirical solutions to this term have been prepared such as those reported in the modified Ergun equation [*Ergun*, 1952]. The viscous energy losses are accounted for by the Kozeny equation for laminar flow, and the kinetic energy losses are described by the Burke-Plummer equation for turbulent flow [*Corapcioglu et al.*, 2004].

[29] This theoretical methodology has been validated with experimental data reported in the literature, including cases that are relevant to the GCS case [*Roosevelt and Corapcioglu*, 1998]. After making one additional substitution for the volume of $CO_2$ (i.e., $V = \frac{4}{3}\pi R_{CO_2}^3$, where $R_{CO_2}$ is the equivalent radius of a sphere with a volume equal to that of a specified bubble), the conservation of momentum equation can be written as

$$\frac{4}{3}\pi R_{CO_2}^3\left(\rho_{matrix}-\rho_{CO_2}\right)g-\frac{4}{3}\pi R_{CO_2}^3 A \cdot\left[\frac{150\mu_{matrix}u(1-\phi)^2}{d_P^2\phi^3}+\frac{1.75\rho_{CO_2}u^2(1-\phi)}{d_P\phi^3}\right]-2\pi R_P\sigma\sin\theta = \frac{4}{3}\pi R_{CO_2}^3\left(\rho_{CO_2}+C_M\rho_{matrix}\right)\left(\frac{\partial u}{\partial t}+u\frac{\partial u}{\partial y}\right) \quad (11)$$

The solution to this equation under steady state conditions (i.e., $\frac{Du}{Dt}=0, C_M=0$) is the terminal velocity of $CO_2$ bubble rise under channel or bubbly flow conditions and it can be written as follows [*Corapcioglu et al.*, 2004]:

To illustrate how the rise velocity of leaked $CO_2$ would behave in response to the viscosity measurements made here, equation (12) was solved for the two leakage pathways presented in Figure 1. The characteristics for two representative geologic formations are also selected to understand the relative importance of geothermal gradients (Table 3) as compared to porosity, pore throat, particle size, and $CO_2$ bubble size (Table 4).

[30] The results, shown in Figure 15, demonstrate how rapidly rise velocity decreases with increases in matrix viscosity. For both geologic formations modeled here, an increase in viscosity from 0.65 to 5.42 mPa·s can slow the terminal velocity up to 90%. The rise velocity under geological condition 2, which represents coarse porous media, is about two orders of magnitude higher than that under geological condition 1, with all the other conditions remaining the same. Buoyancy has a much weaker effect on the rise velocity. Stronger buoyancy (leakage pathway a compared to leakage pathway b) increases the rise velocity only slightly. The extent of influence of buoyancy on the rise velocity varies with a more pronounced effect under the regime of fine porous media (geological condition 1) and with an insignificant effect under the regime of coarse porous media (geological condition 2). These results suggest that under realistic conditions, the viscosity of the matrix fluid affects the rise velocity independently of the geological, geothermal, and hydrostatic

$$u=\frac{\mu_{matrix}(1-\phi)}{\rho_{CO_2}d_P}\left[-42.857+\sqrt{1836.74-\frac{0.57}{A}\left(\frac{\rho_{CO_2}d_P^3\phi^3}{\mu_{matrix}^2(1-\phi)^3}\right)\left(\frac{1.5R_P\sigma\sin\theta}{R_{CO_2}^3}-\left(\rho_{matrix}-\rho_{CO_2}\right)g\right)}\right] \quad (12)$$

**Table 4.** Geological Properties Used in Equation (12)

| Parameter | Geological Condition 1 | Geological Condition 2 | Reference |
|---|---|---|---|
| Average porosity, $\overline{\phi}$(%) | 0.2386 | 0.3954 | [*Al-Raoush and Willson*, 2005; *Chen et al.*, 2003; *Padhy et al.*, 2007; *Widjajakusuma et al.*, 1999] |
| Average particle size, $\overline{d_p}$ (m) | 0.0025 | 0.004 | [*Corapcioglu et al.*, 2004; *Glover and Walker*, 2011; *Peters*, 2009] |
| Average pore throat, $\overline{R_p}$ (m) | 0.001 | 0.0028 | [*Chen et al.*, 2003; *Padhy et al.*, 2007; *Song*, 2001] |
| Average bubble radius, $\overline{R_{CO_2}}$ (m) | 0.0015 | 0.003 | Experimental data |

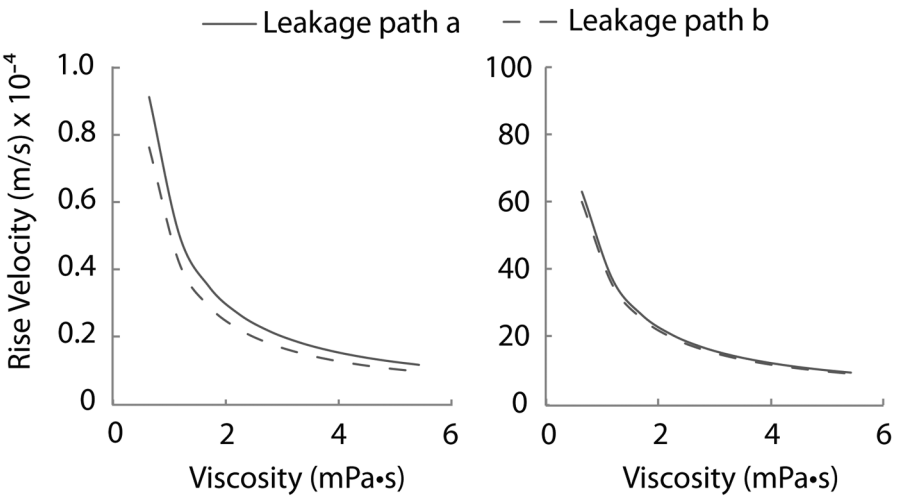


**Figure 15.** Rise velocity of leaked $CO_2$ channel or bubbly flow through porous media obtained from equation (12) using the viscosity data measured in this work following the two leakage pathways defined in Figure 1, under two specified geological conditions: (left) geological condition 1 for fine porous media; (right) geological condition 2 for coarse porous media. The characteristics of these geological conditions are listed in Table 4.

conditions while the impact from buoyancy is more case specific.

## 5. Summary and Conclusions

[31] Together, the results of this work help paint a more complete picture of flow properties that are likely to influence the leakage processes that will impact the feasibility of geologic carbon sequestration. In particular, the results demonstrate that the ebullition and evolution of $CO_{2(g)}$ bubbles could act to impede vertical flow of $CO_2$-brine mixtures through porous formations in as much as these bubbles will alter the effective viscosity of the mixture. The change in the viscosity will influence the force balance on a rising bubble of $CO_2$. and this will have important implications for developing more accurate estimates of residence time that $CO_2$ and brines will spend in contact with specific formations for investigating reaction kinetics and other associated processes. Further, this work cataloged the effect of shear, ionic strength, pressure, and temperature on the flow properties of these $CO_2$-brine mixtures. Existing models of complex multiphase flow were found to adequately predict how these mixtures will behave over a range of conditions. Finally, the experimental results demonstrate that the microstructure that results under VLE conditions in $CO_2$-brine mixtures is strongly influenced by shear and that the bubbles are easily disrupted. This work combined experimental results with applicable modeling frameworks to provide a first look at how $CO_2$ would travel over long distances. These results could aid in more thorough characterization of possible repositories. When assessing the viability of a potential GCS site, the thermal gradient in the subsurface must be considered together with specific formation characteristics (e.g., water saturation, permeability, porosity, stratification, etc.) and connate brine properties (e.g., ionic strength, pH) to develop a better understanding of how $CO_2$ might escape.

[32] **Acknowledgments.** The authors thank Brian Tison and Jasmine Copeland for their assistance in data collection. This work was funded by the University of Virginia School of Engineering and Applied Science through faculty start-up funds as well as through the National Science Foundation (grant CBET-1134397).

## References

Adamson, A. W. (1997), *Physical Chemistry of Surfaces*, 6th ed., Wiley, New York.

Al-Raoush, R. I., and C. S. Willson (2005), Extraction of physically realistic pore network properties from three-dimensional synchrotron X-ray microtomography images of unconsolidated porous media systems, *J. Hydrol.*, *300*(1–4), 44–64, doi:10.1016/j.jhydrol.2004.05.005.

Bachu, S., and J. J. Adams (2003), Sequestration of $CO_2$ in geological media in response to climate change: Capacity of deep saline aquifers to sequester $CO_2$ in solution, *Energy Convers. Manage.*, *44*(20), 3151–3175, doi:10.1016/S0196-8904(03)00101-8.

Bachu, S., and D. Brant Bennion (2009), Dependence of $CO_2$-brine interfacial tension on aquifer pressure, temperature and water salinity, *Energy Procedia*, *1*(1), 3157–3164, doi:10.1016/j.egypro.2009.02.098.

Bando, S., F. Takemura, M. Nishio, E. Hihara, and M. Akai (2003), Solubility of $CO_2$ in aqueous solutions of NaCl at (30 to 60)°C and (10 to 20) MPa, *J. Chem. Eng. Data*, *48*(3), 576–579, doi:10.1021/je0255832.

Bando, S., F. Takemura, M. Nishio, E. Hihara, and M. Akai (2004), Viscosity of aqueous NaCl solutions with dissolved $CO_2$ at (30 to 60)°C and (10 to 20) MPa, *J. Chem. Eng. Data*, *49*(5), 1328–1332, doi:10.1021/je049940f.

Barnes, H. A. (1997), Thixotropy–A review, *J. Non-Newtonian Fluid Mech.*, *70*(1–2), 1–33, doi:10.1016/S0377-0257(97)00004-9.

Benson, S. M., and D. R. Cole (2008), $CO_2$ Sequestration in Deep Sedimentary Formations, *Elements*, *4*(5), 325–331, doi:10.2113/gselements.4.5.325.

Birkholzer, J. T., and Q. Zhou (2009), Basin-scale hydrogeologic impacts of $CO_2$ storage: Capacity and regulatory implications, *Int. J. Greenh. Gas Control*, *3*(6), 745–756, doi:10.1016/j.ijggc.2009.07.002.

Chen, C., and D. Zhang (2010), Pore-scale simulation of density-driven convection in fractured porous media during geological $CO_2$ sequestration, *Water Resour. Res.*, *46*(11), W11527, doi:10.1029/2010WR009453.

Chen, Q., M. K. Gingras, and B. J. Balcom (2003), A magnetic resonance study of pore filling processes during spontaneous imbibition in Berea sandstone, *J. Chem. Phys.*, *119*, 9609–9616, doi:10.1063/1.1615757.

Chhabra, R. P., and J. F. Richardson (2008), *Non-Newtonian flow and applied rheology engineering applications 2nd ed.*, Butterworth-Heinemann/Elsevier, Boston.

Chiquet, P., J.-L. Daridon, D. Broseta, and S. Thibeau (2007), $CO_2$/water interfacial tensions under pressure and temperature conditions of $CO_2$ geological storage, *Energy Convers. Manage.*, *48*(3), 736–744, doi:10.1016/j.enconman.2006.09.011.

Cihan, A., and M. Y. Corapcioglu (2008), Effect of compressibility on the rise velocity of an air bubble in porous media, *Water Resour. Res.*, *44*(4), W04409, doi:10.1029/2006WR005415.

Corapcioglu, M. Y., A. Cihan, and M. Drazenovic (2004), Rise velocity of an air bubble in porous media: Theoretical studies, *Water Resour. Res.*, *40*(4), W04214, doi:10.1029/2003WR002618.

Crandell, L. E., B. R. Ellis, and C. A. Peters (2010), Dissolution potential of $SO_2$ co-injected with $CO_2$ in geologic sequestration, *Environ. Sci. Technol.*, *44*(1), 349–355, doi:10.1021/es902612m.

Djéridi, H., J. F. Favé, J. Y. Billard, and D. H. Fruman (1999), Bubble capture and migration in Couette–Taylor flow, *Exp. Fluids*, *26*(3), 233–239, doi:10.1007/s003480050284.

Dooley, J., R. Dahowski, C. Davidson, M. Wise, N. Gupta, S. Kim, and E. L. Malone (2006), Carbon dioxide capture and geologic storage—A core element of a global energy technology strategy to address climate change, in *Joint Global Change Research Institute (JGCRI)*, pp. 37, Battelle Memorial Institute, College Park Md.

Duan, Z., R. Sun, C. Zhu, and I. M. Chou (2006), An improved model for the calculation of $CO_2$ solubility in aqueous solutions containing $Na^+$, $K^+$, $Ca^{2+}$, $Mg^{2+}$, $Cl^-$, and $SO_4^{2-}$, *Mar. Chem.*, *98*(2–4), 131–139, doi:10.1016/j.marchem.2005.09.001.

Eccles, J. K., L. Pratson, R. G. Newell, and R. B. Jackson (2009), Physical and economic potential of geological $CO_2$ storage in saline aquifers, *Environ. Sci. Technol.*, *43*(6), 1962–1969, doi:10.1021/es801572e.

Ergun, S. (1952), Mass-transfer rate in packed columns, *Chem. Eng. Prog.*, *48*, 89–94.

Espinoza, D. N., and J. C. Santamarina (2010), Water-$CO_2$-mineral systems: Interfacial tension, contact angle, and diffusion—Implications to $CO_2$ geological storage, *Water Resour. Res.*, *46*(7), W07537, doi:10.1029/2009WR008634.

Garcia, J. E. (2001), Density of aqueous solutions of $CO_2$, Lawrence Berkeley Natl. Lab., Oak Ridge, Tenn.

Gasda, S. E., J. M. Nordbotten, and M. A. Celia (2011), Vertically averaged approaches for $CO_2$ migration with solubility trapping, *Water Resour. Res.*, *47*(5), W05528, doi:10.1029/2010WR009075.

Glover, P. W. J., and Walker, E. (2011), Grain-size to effective pore-size transformation derived from electrokinetic theory, *Geophysics*, *76*(4), 17–29.

Hebach, A., A. Oberhof, N. Dahmen, A. Kögel, H. Ederer, and E. Dinjus (2002), Interfacial tension at elevated pressures measurements and correlations in the water + carbon dioxide system, *J. Chem. Eng. Data*, *47*(6), 1540–1546, doi:10.1021/je025569p.

IPCC (2005), *Carbon Dioxide Capture and Storage*, Intergovernmental Panel on Climate Change, Geneva, Switzerland.

Joh, S. W., S. H. Lee, and J. R. Youn (2010), Rheological behavior of polydispersed bubble suspensions in shear flows, *Polym. Eng. Sci.*, *50*(1), 128–137, doi:10.1002/pen.21517.

Juanes, R., E. J. Spiteri, F. M. Orr Jr., and M. J. Blunt (2006), Impact of relative permeability hysteresis on geological $CO_2$ storage, *Water Resour. Res.*, *42*(12), W12418, doi:10.1029/2005WR004806.

Kijevčanin, M. L., V. Z. Kostić, I. R. Radović, B. D. Đorđević, and S. P. Šerbanović (2008), Viscosity of binary non-electrolyte liquid mixtures: Prediction and correlation, *Chem. Ind. Chem. Eng. Q.*, *14*(4), 223–226, doi:10.2298/CICEQ0804223K.

Klempner, D., and K. C. Frisch (1991), *Handbook of Polymeric Foams and Foam Technology*, Hanser, New York.

Kloek, W., T. van Vliet, and M. Meinders (2001), Effect of bulk and interfacial rheological properties on bubble dissolution, *J. Colloid Interface Sci.*, *237*(2), 158–166, doi:10.1006/jcis.2001.7454.

Kneafsey, T. J., and K. Pruess (2010), Laboratory flow experiments for visualizing carbon dioxide-induced, density-driven brine convection, *Transp. Porous Media*, *82*(1), 123–139, doi:10.1007/s11242-009-9482-2.

Kumagai, A., and C. Yokoyama (1998), Falling capillary tube viscometer suitable for liquids at high pressure, *Rev. Sci. Instrum.*, *69*, 1441–1445, doi:10.1063/1.1148778.

Kumagai, A., and C. Yokoyama (1999), Viscosities of aqueous NaCl solutions containing $CO_2$ at high pressures, *J. Chem. Eng. Data*, *44*(2), 227–229, doi:10.1021/je980178p.

Kumar, P. P., A. G. Kalinichev, and R. J. Kirkpatrick (2009), Hydrogen-bonding structure and dynamics of aqueous carbonate species from Car-Parrinello molecular dynamics simulations, *J. Phys. Chem. B*, *113*(3), 794–802, doi:10.1021/jp809069g.

Lackner, K. S. (2003), A guide to $CO_2$ sequestration, *Science*, *300*(5626), 1677–1678, doi:10.1126/science.1079033.

Laliberté, M. (2007), Model for calculating the viscosity of aqueous solutions, *J. Chem. Eng. Data*, *52*(2), 321–335, doi:10.1021/je0604075.

Li, L., C. A. Peters, and M. A. Celia (2006), Upscaling geochemical reaction rates using pore-scale network modeling, *Adv. Water Resour.*, *29*(9), 1351–1370, doi:10.1016/j.advwatres.2005.10.011.

Llewellin, E. W., and M. Manga (2005), Bubble suspension rheology and implications for conduit flow, *J. Volcanol. Geotherm. Res.*, *143*(1–3), 205–217, doi:10.1016/j.jvolgeores.2004.09.018.

Llewellin, E. W., H. M. Mader, and S. D. R. Wilson (2002a), The rheology of a bubbly liquid, *Proc. R. So. Lond. Ser. A*, *458*(2020), 987–1016.

Llewellin, E. W., H. M. Mader, and S. D. R. Wilson (2002b), The constitutive equation and flow dynamics of bubbly magmas, *Geophys. Res. Lett.*, *29*(24), 2170, doi:10.1029/2002GL015697.

Manga, M., and M. Loewenberg (2001), Viscosity of magmas containing highly deformable bubbles, *J. Volcanol. Geotherm. Res.*, *105*(1–2), 19–24, doi:10.1016/S0377-0273(00)00239-0.

McGinnis, D. F., J. Greinert, Y. Artemov, S. E. Beaubien, and A. Wuest (2006), Fate of rising methane bubbles in stratified waters: How much methane reaches the atmosphere?, *J. Geophys. Res.*, *111*, C09007, doi:10.1029/2005JC003183.

Murai, Y., and H. Oiwa (2008), Increase of effective viscosity in bubbly liquids from transient bubble deformation, *Fluid Dyn. Res.*, *40*(7–8), 565–575, doi:10.1016/j.fluiddyn.2007.12.009.

Nakken, T., M. Tande, and A. Elgsaeter (2001), Measurements of polymer induced drag reduction and polymer scission in Taylor flow using standard double-gap sample holders with axial symmetry, *J. Non-Newtonian Fluid Mech.*, *97*(1), 1–12, doi:10.1016/S0377-0257(00)00195-6.

Nordbotten, J. M., M. A. Celia, S. Bachu, and H. K. Dahle (2005), Semianalytical solution for $CO_2$ leakage through an abandoned well, *Environ. Sci. Technol.*, *39*(2), 602–611, doi:10.1021/es035338i.

Oldenburg, C. M. (2007), Migration mechanisms and potential impacts of $CO_2$ leakage and seepage, in *Carbon Capture and Storage*, edited by E. Wilson and D. Gerard, Blackwell Publ., Ames, IA, 127–146.

Oldenburg, C. M., and J. L. Lewicki (2006), On leakage and seepage of $CO_2$ from geologic storage sites into surface water, *Environ. Geol.*, *50*(5), 691–705, doi:10.1007/s00254-006-0242-0.

Oldenburg, C., J. Lewicki, L. Pan, L. Dobeck, and L. Spangler (2010), Origin of the patchy emission pattern at the ZERT $CO_2$ release test, *Environ. Earth Sci.*, *60*(2), 241–250, doi:10.1007/s12665-009-0442-5.

Padhy, G. S., C. Lemaire, E. S. Amirtharaj, and M. A. Ioannidis (2007), Pore size distribution in multiscale porous media as revealed by DDIF–NMR, mercury porosimetry and statistical image analysis, *Colloids Surf. A*, *300*(1–2), 222–234, doi:10.1016/j.colsurfa.2006.12.039.

Patzek, T. W., D. B. Silin, S. M. Benson, and G. I. Barenblatt (2003), On vertical diffusion of gases in a horizontal reservoir, *Transp. Porous Media*, *51*(2), 141–156, doi:10.1023/A:1021957416536.

Peters, C. A. (2009), Accessibilities of reactive minerals in consolidated sedimentary rock: An imaging study of three sandstones, *Chem. Geol.*, *265*(1–2), 198–208, doi:10.1016/j.chemgeo.2008.11.014.

Poletto, M., and D. D. Joseph (1995), The effect of density and viscosity of a suspension, *J. Rheol.*, *39*(2), 323–343.

Pollak, M. F., and E. J. Wilson (2009), Regulating geologic sequestration in the United States: Early rules take divergent approaches, *Environ. Sci. Technol.*, *43*(9), 3035–3041, doi:10.1021/es803094f.

Pruess, K. (2008a), On $CO_2$ fluid flow and heat transfer behavior in the subsurface, following leakage from a geologic storage reservoir, *Environ. Geol.*, *54*(8), 1677–1686, doi:10.1007/s00254-007-0945-x.

Pruess, K. (2008b), Leakage of $CO_2$ from geologic storage: Role of secondary accumulation at shallow depth, *Int. J. Greenh. Gas Control*, *2*(1), 37–46, doi:10.1016/S1750-5836(07)00095-3.

Riaz, A., and H. A. Tchelepi (2008), Dynamics of vertical displacement in porous media associated with $CO_2$ sequestration, *SPE J.*, *13*(3), 305–313, doi:10.2118/103169-PA.

Roosevelt, S. E., and M. Y. Corapcioglu (1998), Air bubble migration in a granular porous medium: Experimental studies, *Water Resour. Res.*, *34*(5), 1131–1142, doi:10.1029/98WR00371.

Sang-Yoon, K., S. S. Ashok, T. Heng-Kwong, and L. K. Donald (1997), Rheology of dense bubble suspensions, *Physics of Fluids*, *9*(6), 1540–1561.

Silin, D., T. W. Patzek, and S. M. Benson (2009), A one-dimensional model of vertical gas plume migration through a heterogeneous porous medium, *Int. J. Greenh. Gas Control*, *3*(3), 300–310, doi:10.1016/j.ijggc.2008.09.003.

Sochi, T. (2010), Flow of non-newtonian fluids in porous media, *J. Polym. Sci., B, Polym. Phys.*, *48*(23), 2437–2767, doi:10.1002/polb.22144.

Soli, A. L., and R. H. Byrne (2002), $CO_2$ system hydration and dehydration kinetics and the equilibrium $CO_2/H_2CO_3$ ratio in aqueous NaCl solution, *Mar. Chem.*, *78*(2–3), 65–73, doi:10.1016/S0304-4203(02)00010-5.

Song, Y.-Q. (2001), Pore sizes and pore connectivity in rocks using the effect of internal field, *Magn. Reson. Imaging*, *19*(3–4), 417–421, doi:10.1016/S0730-725X(01)00259-4.

Soubiran, J., and J. D. Sherwood (2000), Bubble motion in a potential flow within a Venturi, *Int. J. Multiphase Flow*, *26*(11), 1771–1796, doi:10.1016/S0301-9322(99)00113-5.

Span, R., E. W. Lemmon, R. T. Jacobsen, W. Wagner, and A. Yokozeki (2000), A reference equation of state for the thermodynamic properties of nitrogen for temperatures from 63.151 to 1000 K and pressures to 2200 MPa, *J. Phys. Chem. Ref. Data*, *29*(6), 1361–1433, doi:10.1063/1.1349047.

Tewes, F., and F. Boury (2005), Formation and rheological properties of the supercritical $CO_2$–water pure interface, *J. Phys. Chem. B*, *109*, 3990–3997, doi:10.1021/jp046019w.

Thompson, M. J., J. R. A. Pearson, and M. R. Mackley (2001), The effect of droplet extension on the rheology of emulsions of water in alkyd resin, *J. Rheol.*, *45*(6), 1341–1358, doi:10.1122/1.1410371.

Tomida, D., A. Kumagai, and C. Yokoyama (2007), Viscosity measurements and correlation of the squalane + $CO_2$ mixture, *Int. J. Thermophys.*, *28*(1), 133–145.

Wallis, G. B. (1969), *One-Dimensional Two-Phase Flow*, 408 pp., McGraw-Hill, New York.

Widjajakusuma, J., B. Biswal, and R. Hilfer (1999), Quantitative prediction of effective material properties of heterogeneous media, *Comput. Mater. Sci.*, *16*(1–4), 70–75, doi:10.1016/S0927-0256(99)00047-6.

Wollenweber, J., S. Alles, A. Busch, B. M. Krooss, H. Stanjek, and R. Littke (2010), Experimental investigation of the $CO_2$ sealing efficiency of caprocks, *Int. J. Greenh. Gas Control*, *4*(2), 231–241, doi:10.1016/j.ijggc.2010.01.003.

Yang, C., and Y. Gu (2006), Accelerated mass transfer of $CO_2$ in reservoir brine due to density-driven natural convection at high pressures and elevated temperatures, *Ind. Eng. Chem. Res.*, *45*(8), 2430–2436, doi:10.1021/ie050497r.

Zafarani-Moattar, M. T., and R. Majdan-Cegincara (2009), Viscosity modeling and prediction of aqueous mixed electrolyte solutions, *Ind. Eng. Chem. Res.*, *48*(12), 5833–5844, doi:10.1021/ie801933u.

Zhang, J., and L.-S. Fan (2003), On the rise velocity of an interactive bubble in liquids, *Chem. Eng. J.*, *92*(1–3), 169–176, doi:10.1016/S1385-8947(02)00189-4.

Zhang, Y., C. M. Oldenburg, S. Finsterle, P. Jordan, and K. Zhang (2009), Probability estimation of $CO_2$ leakage through faults at geologic carbon sequestration sites, *Energy Procedia*, *1*(1), 41–46, doi:10.1016/j.egypro.2009.01.008.